HHS Public Access

Author manuscript

J Mol Biol. Author manuscript; available in PMC 2016 September 25.

Published in final edited form as:

J Mol Biol. 2015 September 25; 427(19): 3096–3109. doi:10.1016/j.jmb.2015.07.024.

The LcrG tip chaperone protein of the *Yersinia pestis* type III secretion system is partially folded

Sukanya Chaudhury[1], **Clarice de Azevedo Souza**[2], **Gregory V. Plano**[2], and **Roberto N. De Guzman**[1,*]

[1]Department of Molecular Biosciences, University of Kansas, Lawrence, KS 66045 USA

[2]Department of Microbiology and Immunology, University of Miami Miller School of Medicine, 1600 N.W. 10th Ave, Miami, FL 33136 USA

Abstract

The type III secretion system (T3SS) is essential in the pathogenesis of *Yersinia pestis*, the causative agent of plague. A small protein, LcrG, functions as a chaperone to the tip protein LcrV, and the LcrG-LcrV interaction is important in regulating protein secretion through the T3SS. The atomic structure of the LcrG family is currently unknown. However, because of its predicted helical propensity, many have suggested that the LcrG family forms a coiled-coil structure. Here, we show by NMR and CD spectroscopy that LcrG lacks a tertiary structure and it consists of three partially folded alpha helices spanning residues 7-38, 41-46, and 58-73. NMR titrations of LcrG with LcrV show that the entire length of a truncated LcrG (residues 7-73) is involved in binding to LcrV. However, there is regional variation in how LcrG binds to LcrV. The C-terminal region of a truncated LcrG (residues 52-73) shows tight-binding interaction with LcrV while the N-terminal region (residues 7-51) shows weaker interaction with LcrV. This suggests there are at least two binding events when LcrG binds to LcrV. Biological assays and mutagenesis indicate that the C-terminal region of LcrG (residues 52-73) is important in blocking protein secretion through the T3SS. Our results reveal structural and mechanistic insights into the atomic conformation of LcrG and how it binds to LcrV.

Graphical Abstract

Correspondence to Roberto N. De Guzman: rdguzman@ku.edu.

NMR ASSIGNMENTS

The NMR assignments for LcrG in the free and complex forms have been deposited in the BMRB with accession number 26592.

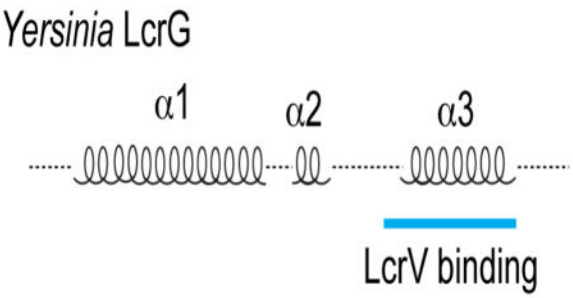

Keywords

LcrG; *Yersinia pestis*; T3SS; NMR; tip chaperone

INTRODUCTION

Pathogenesis of *Yersinia pestis* requires the assembly of the type III secretion system (T3SS) to inject Yops (*Yersinia* outer proteins) into macrophages and other phagocytes to disable the host immune response against infection [1,2]. There are three components of the T3SS – *(i)* structural proteins that assemble into a nanoinjector-like devise consisting of a base, an external needle, and a tip complex; *(ii)* effector proteins that are injected into the host cells to modulate their response to bacterial infection; and *(iii)* chaperone proteins that bind structural and effector proteins prior to secretion [3–6]. In *Y. pestis*, the tip complex is formed by several copies of LcrV (320 residues) [7]. Prior to secretion, the tip protein LcrV is chaperoned by a smaller protein, LcrG (95 residues) [8,9].

LcrG interacts with LcrV [8–14] with nanomolar binding affinity (k_d = 140 nM by SPR) [12]. The N-terminus of LcrG is involved in the binding interaction with LcrV based on results from yeast two hybrid assays [13]. The tight binding interaction of LcrG with LcrV is involved in regulating Yop secretion [15–17]. LcrG functions as a negative regulator of secretion as increased levels of LcrG block Yop secretion [9,16]. The crystal structures of LcrV [18,19] show an overall “dumbbell-shaped” molecule with a central coiled-coil connecting an N-terminal globular domain and a less structured mixed α/β domain. However, the atomic structure of LcrG or any member of the LcrG family of tip chaperones (Fig. 1) is unknown as well as the atomic structure of the LcrG-LcrV. The predicted helical propensity of LcrG (Fig. 1) led others to suggest that LcrG forms a coiled-coil [12,20] and that binding to LcrV involves an LcrG coiled-coil [12]. Others suggested that binding to LcrV involves the formation of an LcrG alpha-helical hairpin [21]. Recently, Basu *et al*. [22] reported a 3D coiled-coil structure for the LcrG homolog in *Pseudomonas aeruginosa*, PcrG, derived by computational modeling. Thus, the current understanding in the literature is that the LcrG family of proteins has a three-dimensional coiled-coil structure [12,20,22].

Here, we show by NMR that unbound LcrG lacks a tertiary structure and that it contains only two partially formed alpha helices. We show that the entire length of LcrG residues 7-73 is involved in binding LcrV. We also identify a short region of LcrG from residues 52-73 that forms a tight interaction with LcrV, while the rest of LcrG residues 7-51 is

involved in weaker interactions with LcrV, suggesting there are at least two binding events when LcrG binds LcrV.

RESULTS

Expression and purification of LcrG

Secondary structure prediction using PSIPRED [23] suggested that the LcrG family of tip protein chaperones was predominantly helical in secondary structures (Fig. 1). Based on the predicted secondary structures of LcrG (Fig. 1), three constructs were expressed and purified for structural characterization: *(i)* the full length LcrG ($LcrG^{FL}$, 95 amino acids), *(ii)* a truncated form spanning residues 7-73 ($LcrG^{7-73}$) that eliminated the predicted random coil regions at the amino and carboxy termini of LcrG, and *(iii)* a C34S point mutation engineered into $LcrG^{7-73}$ (herein referred to as LcrG*). These three LcrG constructs were expressed in soluble forms in *E. coli* as GB1 fusion proteins, digested with tobacco etch virus (TEV) protease and purified under native conditions generating millimolar amounts of purified proteins.

CD spectroscopy

Results of CD spectroscopy confirmed the predominantly helical secondary structure of LcrG (Fig. 2). CD spectra of $LcrG^{FL}$, $LcrG^{7-73}$ and LcrG* showed that the LcrG constructs were primarily α-helical in secondary structure as indicated by the characteristic minima at 222 and 208 nm. The ratios of ellipticities at 222 and 208 nm ($\theta_{222}/\theta_{208}$) were 0.8 for $LcrG^{FL}$ and $LcrG^{7-73}$; and 0.7 for LcrG*, which suggested non-interacting alpha helices [24,25] in contrast to $\theta_{222}/\theta_{208}$ ratio of 1.0 found in helical bundles and coiled-coils [26,27] with extensive interhelical contacts. Comparison of all three CD spectra confirmed that $LcrG^{FL}$ and $LcrG^{7-73}$ had nearly identical secondary structures, and that the C34S mutation did not significantly alter the secondary structure of LcrG (Fig. 2). CD thermal denaturation curves of $LcrG^{FL}$, $LcrG^{7-73}$ and LcrG* showed that all three proteins unfolded in a non-cooperative manner without displaying a clear inflection point (Fig. 2). Overall, the CD data suggests the presence of non-interacting alpha helices in LcrG, or in other words, that LcrG contains secondary structures but lacks a tertiary fold.

NMR spectroscopy

NMR spectroscopy was used to identify the helical regions of LcrG. Full length LcrG ($LcrG^{FL}$) showed poor quality 2D ^{1}H-^{15}N HSQC spectrum (Fig. 3a) that was characterized by overlapped peaks; poor dispersion and resolution; and less peaks than expected for a 95-residue protein. The poor quality of the ^{15}N HSQC of $LcrG^{FL}$ made it unsuitable for further NMR characterization. We reasoned that the poor quality of the NMR spectrum of $LcrG^{FL}$ could be due to the presence of a native cysteine at position 34 that might form disulfide linkages and contribute to the aggregation of the protein, which could result in the broadened peaks seen in Fig. 3a. Mutation of C34 into serine somewhat improved the NMR spectrum (Fig. 3b), however the 2D ^{1}H-^{15}N HSQC spectrum of $LcrG^{FL}$ C34S was also non-ideal for further NMR characterization because of the significant number of overlapping peaks and conformational heterogeneity (Fig. 3b), which possibly arose from the cis-trans isomerization of the prolines present in the flexible C-terminal tail of LcrG. Truncation of

the predicted disordered tails to form the LcrG$^{7-73}$ construct improved the 2D ^{1}H-^{15}N HSQC spectrum but did not result in an ideal NMR spectrum either. Only 58% of the residues in the protein were represented in the 2D ^{1}H-^{15}N HSQC spectrum of LcrG$^{7-73}$ and the peaks were broad and poorly resolved (Fig. 3c). Mutation of C34 in the LcrG$^{7-73}$ construct to alanine (Fig. 3d) or serine (Fig. 4) significantly improved the quality of the NMR data; however, the 2D ^{1}H-^{15}N HSQC spectrum of the C34A mutant (Fig. 3d) still exhibited broad and overlapping peaks. In contrast, the C34S mutation yielded an excellent quality 2D ^{1}H-^{15}N HSQC spectrum with sharp and well-resolved peaks (Fig. 4). Thus, LcrG* (or LcrG$^{7-73}$ C34S) was deemed the best construct for further NMR characterization.

NMR backbone assignments

Three-dimensional NMR datasets were acquired using ^{15}N/^{13}C LcrG* for backbone resonance assignments. Of the 67 backbone amides of LcrG*, 62 were assigned (Fig. 4). The backbone amides of H25, R26, E32, M45, and K46 could not be assigned due to rapid solvent exchange or exchange dynamics on the us-ms time scale. The overlapping peaks are indicated in Fig. 4 with asterisks. The backbone resonances of I37, I47, and F48 were assigned by ^{15}N amino acid specific labeling and by introducing an I37A point mutation in LcrG*.

The secondary ^{13}Cα and ^{13}Cβ chemical shifts of LcrG* suggested three α-helical regions spanning residues 7-38, 41-46, and 58-73 (designated helix α1-α3 in Fig. 5). Regions with consecutive residues of positive ^{13}Cα secondary chemical shifts were assigned as alpha helical [28]. Helix α1 showed somewhat lower ^{13}Cα secondary chemical shifts compared to helix α2 and α3. The helices were linked by a short 2-residue linker (residue 39-40) between helix α1 and helix α2 and a 10-residue linker (residue 47-56) between helix α2 and α3. Although residue 57 near helix α3 showed a positive ^{13}Cα secondary chemical shift, we assigned helix α3 to begin with a proline residue, P58, because a proline being a helix breaker is less likely found within a helix but can be found at the beginning of a helix [29]. Likewise, helix α2 begins with another proline, P41. Using the method of Eliezer *et al.* [30] in estimating the fractional helicity based on ^{13}Cα secondary chemical shifts and assuming a simple (unfolded ↔ folded) two state model and a ^{13}Cα secondary chemical shift value of 3.1 for a fully formed helix [31]), the estimated fraction of formed helix α1, α2, and α3 in LcrG is 36%, 63%, and 50%, respectively (Supplementary Information Fig. S1). In other words, the fractional helicity of the three helices of LcrG is not uniform – helix α2 is relatively the most formed helix, while helix α1 is the least formed helix of LcrG.

LcrG backbone dynamics

The steady state heteronuclear {^{1}H}-^{15}N NOE and ^{15}N backbone relaxation rates (R_1 and R_2) were acquired to assess the backbone dynamics of LcrG*. The heteronuclear {^{1}H}-^{15}N NOEs provide a measure of fast backbone dynamics at the picosecond to nanosecond time scale and the values of {^{1}H}-^{15}N NOEs qualitatively describe backbone flexibility. Heteronuclear {^{1}H}-^{15}N NOE values above 0.6 are found in residues that form well-ordered structures and can be comparatively described as having rigid backbone flexibility; values below 0.2 have random coil flexibility; and those between 0.4–0.6 have semi-rigid flexibility. The extreme terminal residues of LcrG* (D7 and R73) showed random coil

flexibility with {^{1}H}-^{15}N NOE values below 0.2 (Fig. 6a). Most of the residues in the α-helices showed semi-rigid flexibility with {^{1}H}-^{15}N NOEs values between 0.4–0.6 (Fig. 6a). There were a few residues in the beginning of α-helix 1 (E8, D10, K11, K14, Ala-19) and one in the extreme end of helix α3 (E72) that displayed higher flexibility as indicated by their {^{1}H}-^{15}N NOE values of below 0.4 (Fig. 6a). There were also residues in all the three α-helices (K28, L29, Ala-43, E66 and R69) with {^{1}H}-^{15}N NOE values above 0.6 suggesting these residues have backbone flexibility approaching those found in well-ordered protein structures. Additionally, residues at the linker regions between the helices displayed {^{1}H}-^{15}N NOE values above 0.4, suggesting these loop regions are not random coil in flexibility but have backbone flexibility similar to the helical regions.

The ^{15}N backbone relaxation rates (R_1 and R_2) indicated that the α-helices behaved with nearly similar backbone dynamics. There were no drastic changes in the R_1 rates throughout the entire length of LcrG* suggesting that the protein, despite not having a well-ordered structure, tumbles as a single unit similar to what is observed for R_1's of well-ordered protein domains. Regarding the R_2 rates, residues 50-53 within the linker region between helix α2 and helix α3 showed a uniform decrease in R_2 and an increase in R_1 (Fig. 6b and Fig. 6c). The penultimate residue of helix α1 (I37) and the linker residue K57 showed increased R_2 without a corresponding increase in R_1. This suggested chemical exchange on the μs-ms timescale for I37 and K57 (Fig. 6b and Fig. 6c). Excluding these two residues, the R_2 relaxation rates remained almost uniform throughout the protein.

NMR titrations of ^{15}N-labeled LcrG with LcrV

We used NMR chemical shift perturbation to characterize the interaction of LcrG and LcrV. Upon titration with LcrV, the N-terminal $2_{/3}$ of LcrG* from residues 7-51 showed progressive reduction in peak intensities indicating complex formation at an intermediate exchange time scale (Fig. 7a). The remaining C-terminal $1_{/3}$ of LcrG*, from residues 52-73 (except residue 61), were in slow exchange and appeared as new peaks (marked with asterisks in Fig. 7a) upon complex formation. The new slow exchange peaks were identified by 3D NMR datasets using a 1:1.2 molar ratio complex of ^{15}N/^{13}C LcrG* with unlabeled LcrV. The weighted ^{1}H,^{15}N chemical shift perturbations of residues 52-73 are shown in Supplementary Information Fig. S2. Slow exchange peaks are associated with tight-binding interactions (typically with nanomolar k_d), whereas intermediate exchange peaks are associated with weak-binding interactions (typically with micromolar k_d). Thus, NMR titrations suggested that there are two binding events when LcrG* interacts with LcrV. One binding event is characterized by stronger interaction involving the C-terminal LcrG* residues 52-73, and the other binding event is characterized by weaker interaction involving the N-terminal LcrG* residues 7-51.

NMR titrations of ILV-labeled LcrG with LcrV

We used ILV-labeled LcrG* (where the methyl groups of isoleucine, leucine, and valine were ^{13}C-labeled) in NMR titrations with LcrV. We assigned the 5 isoleucine ^{13}Cδ1 methyl groups and the valine ^{13}Cγ methyl groups of LcrG by mutagenesis, however, the leucine methyl groups could not be assigned by mutagenesis because of the significant number of overlapping peaks. Upon titration with LcrV, all the five isoleucines (I20, I37, I47, I56 and

I67) and the lone valine (V44) of LcrG* showed reduction in peak intensities (Fig. 8a and Fig. 8b). In addition, two new slow-exchange peaks appeared in the isoleucine methyl region (Fig. 8a). Results of ^{15}N titration of LcrG* with LcrV (Fig. 7b) showed that the LcrG* region spanning residues 52-73, which contained two isoleucine residues I56 and I67, was in slow-exchange. Thus, the two slow-exchange peaks in the ILV-titration of LcrG with LcrV were most likely I56 and I67. The results of ILV-titration suggested that the methyl groups, hence, hydrophobic contacts, were involved in the LcrG-LcrV complex formation.

NMR titrations of isoleucine ^{13}C-methyl labeled LcrV with LcrG* and LcrG^{FL}

To determine the effect of LcrG truncation with respect to binding to LcrV, LcrV labeled with isoleucine $^{13}C\delta1$ methyl group was titrated with unlabeled LcrG* or LcrG^{FL} C34S. Although the isoleucine $^{13}C\delta1$ methyl groups of LcrV have not been assigned, notably the same set of Ile residues of LcrV were perturbed upon binding to both LcrG* and LcrG^{FL} C34S. In both in LcrG* (Fig. 8c) and LcrG^{FL} C34S (Fig. 8d) there were four peaks that appeared in new positions (Fig. 8c and Fig. 8d), and same peaks underwent significant reduction in intensities. Thus, the truncation of LcrG did not affect the ability of LcrG to bind to LcrV.

Yop secretion assay

A Yop secretion assay was used to evaluate the functional significance of mutations in LcrG. Exogenous LcrG was expressed from a pBad18 vector and assayed for its function in regulating Yop secretion in *Y. pestis.* For wild type LcrG, *Y. pestis* secretes YopM only in the absence of Ca^{2+}, whereas a null LcrG strain (Δ*lcrG*) secretes YopM constitutively in the presence and absence of Ca^{2+}. The LcrG C34S or C34A mutation successfully complemented a Δ*lcrG* null strain of *Y. pestis*, restoring Ca^{+2} regulated secretion of YopM (Fig. 9a), indicating that the LcrG C34S or C34A mutation behaved like wild type LcrG.

Based on the observation from the NMR titration experiments that S52 to R73 of LcrG represented the tight-binding region for complex formation with LcrV, the Yop secretion assay was also used to evaluate the functional significance of this region in *Y. pestis.* The basis for this experiment is that LcrG-LcrV complex formation is necessary for the Ca^{2+}-regulated secretion of YopM [9,13]; whereas disruption of LcrG-LcrV complex formation results in constitutive YopM secretion in the presence or absence of Ca^{2+} [9,13]. The following LcrG mutations were used in the Yop secretion assay: a deletion of the entire region (Δ52-73), four mini deletion mutants (Δ52-57, Δ58-62, Δ63-67 and Δ68-73), and point mutations in I56, K57, R61, L63, I67 and K68. The point mutations were introduced on the basis of secondary structure predictions, which indicated that the region 52-73 formed an amphipathic helix with residues I56, L63, and I67 forming a hydrophobic surface, and on the other face of the helix, residues K57, R61 and K68 forming a hydrophilic surface. Point mutations were designed to alter the hydrophobicity, polarity or charge (i.e. I56N, K57L or K57E). The larger deletion (Δ52-73) and the mini deletions of 4 to 5 residues did not compromise LcrG expression and resulted in constitutive Yop secretion, with the exception of the most C terminal one (Δ68-73). Point mutations within these small deletions did not affect Yop secretion except L63N. The loss or significant decrease in expression of LcrG L63N could potentially result in this loss of calcium regulation. However, with the exception

of L63N all other point mutants showed LcrG expression. The visible band in Fig. 9b with the LcrG antibody used against the ΔLcrG variant is the LcrG(Δ39-53) protein that is expressed from the ΔlcrG on pCD1. These results suggest that deleting 4 to 5 amino acid segments within the region spanning 52-67 is necessary for disrupting the Ca^{2+}-regulated secretion of YopM. Additionally it also suggests that the region 52-67 in LcrG is important in blocking the secretion of Yop effectors.

DISCUSSION

There are currently no atomic structures for any member of the LcrG family (Fig. 1) of tip chaperone proteins. Full length LcrG was unsuitable for NMR studies (Fig. 3), however, a shorter construct, LcrG* ($LcrG^{7-73}$ C34S) lacking the predicted flexible tails was suitable for NMR characterization (Fig. 4). The C34S mutation did not alter the wild type function of LcrG in regulating the Ca^{+2} dependent secretion of YopM in *Y. pestis* (Fig. 9) but it prevented the non-specific oligomerization of LcrG via disulfide bonds that made wild type LcrG unsuitable for NMR studies. The secondary structures of full length LcrG were also present in LcrG* based on CD spectroscopy (Fig. 2). Full length LcrG and LcrG* bound to the same surface of LcrV as suggested by results of NMR titrations using LcrV with ^{13}C-methyl labeled isoleucines as probes (Fig. 8). LcrG* included the minimum region (residues 7-40) that was identified by others to be required for interaction with LcrV [13]. Currently, LcrG* is the most suitable construct for NMR characterization that allows structural insights into the LcrG family of tip chaperones.

The hypothesis in the literature is that LcrG forms a coiled-coil [12,20], however, our CD (Fig. 2) and NMR data (Fig. 5) in combination show that LcrG lacks a tertiary structure and contains only alpha helical secondary structures (Fig. 5). The Cα chemical shifts identified the alpha helical regions of LcrG (Fig. 5). Overall, the α-helices in LcrG were more flexible compared to alpha helices found in proteins with well-defined tertiary structures (Fig. 6). However, there were residues in all the three α-helices whose backbone dynamics approached those seen in more stable helices of proteins with well-defined tertiary structures. Despite lacking a tertiary structure, the helices of LcrG tumble with the same R_1 and R_2 rates (Fig. 6) as opposed to the helices tumbling with different rates or flapping around. This suggests that the interhelical regions of LcrG are not random coil in flexibility. NMR data best describe LcrG as a partially folded alpha helical protein, and its flexibility suggests that crystallization is likely difficult..

The partially folded nature of LcrG is also seen among other T3SS chaperones, where structural disorder specifically contributes to their function [32]. For example, CesAB from the enteropathogenic *E. coli*, a chaperone for the needle filament protein EspA is also an alpha helical protein with a poorly packed helical bundle, like LcrG. Upon binding to EspA, CesAB acquires a well-folded conformation. Interestingly though, stabilization of the conformation of CesAB by correcting the packing defects of the coiled coil, leads to a non-functional T3SS. This example clearly indicates the importance of structural flexibility in achieving function. Additionally other T3SS chaperones like SseA and EscC from different bacterial species also display similar partially folded conformations [32]. Thus, proteins with highly dynamic conformations play important roles in type III secretion. Such intrinsically

flexible proteins are also seen among some effectors and structural proteins of the T3SS [33,34]. Thus, our results add the LcrG tip protein chaperone into the growing list of disordered [33,35] or partially folded [34,36–38] proteins or domains that play important roles in type III secretion. The common theme among these flexible proteins that lack well-defined structures is the disorder-to-order transition when they bind other proteins or their ligands. The conformational dynamics of LcrG perhaps contribute to its functional versatility, which is a characteristic signature of many flexible proteins [39,40]. Indeed LcrG binds to and functions as a chaperone for LcrV as well as a key regulator of type III secretion. The conformationally interchangeable nature of intrinsically flexible structures like LcrG likely ensures easier adaption of distinct transient states which possibly contributes in carrying out multiple roles within the cellular environment.

How LcrG binds to LcrV is poorly understood as there is currently no atomic structure for the LcrG-LcrV complex. Our NMR titrations (Fig. 7) indicate that the entire length of LcrG* residues 7-73 is involved in the interaction with LcrV. Our NMR results preclude a scenario where LcrG forms a coiled-coil upon binding to LcrV as suggested previously [12]. Formation of an LcrG coiled-coil would have resulted in a more dispersed 2D ^{1}H-^{15}N HSQC of LcrG compared to what we had observed (Fig. 7). Further, the secondary $^{13}C\alpha$ secondary chemical shifts of the slow-exchange peaks (residues 52-63) of the complex form of LcrG (Supplementary Information Fig. S3) did not show an increased helicity (Supplementary Information Fig. S1) compared to the free form. Our titration data agrees with the literature that the N-terminus of LcrG is the binding site for LcrV [9,13]. However, our NMR titrations also indicated that the C-terminus of LcrG is involved in binding LcrV (Fig. 7). There can be two primary explanations for this observation. First, it is possible that the sheer difference in size between the two binding partners (37 kDa for LcrV and 8 kDa for LcrG) entails that almost the entire length of the smaller protein (LcrG) is needed to form a stable binding interface. Since LcrG is partially folded and intrinsically flexible, it is highly likely that LcrG entwines around LcrV. This is not uncommon since many flexible proteins present a larger surface area for interaction as compared to globular proteins [39].

The deletion mutants (Δ52-57, Δ58-62, Δ63-67 and Δ52-73) and the one point mutant, L63N showed a defect in the secretion blocking activity of LcrG (Fig. 9). The rest of the point mutants (I56N, K57E, K57L, R61E, R61L, I67N, K68E and K68L) and one deletion mutant, Δ68-73, behaved as wild type LcrG. Thus, NMR results plus the results of the Yop secretion assay suggest that the region S52 to I67 in LcrG plays an important role in blocking the secretion of Yop effectors. Results of Matson and coworkers [13] suggested that the residue F48 in LcrG, is involved in blocking the secretion of Yops. Our results are further corroborated by studies on the homolog, PcrG, which implicated that the C-terminus of PcrG is important in blocking the secretion of effector proteins [41]. Additionally, it is also possible that the LcrV binding and secretion blocking regions of LcrG overlap, and hence none of the mutants could block secretion of YopM.

In summary, NMR and CD data show that LcrG is a partially folded α-helical protein that lacks a tertiary structure, and that the entire length of LcrG residues 7-73 is involved in the interaction with LcrV.

MATERIALS AND METHODS

Protein expression and purification

The coding regions of *Y. pestis* $LcrG^{FL}$ (full length version spanning residues 1-95) and $LcrG^{7-73}$ (the truncated form spanning residues 7-73) were PCR amplified from pCD1 [42] and subcloned into the pET-21a expression vector using NdeI and BamHI as the restriction sites. The vector was modified to encode an N-terminal His_6-tagged GB1 domain followed by a tobacco etch virus (TEV) protease site. GB1 (56 residues) is the B1 immunoglobulin binding domain from *Streptococcus* protein G that functions as a solubility enhancement tag [43,44]. For protein expression, plasmids were transformed in *E. coli* BL21 (DE3) DNAY cells and colonies were picked to inoculate a starter culture of 50 mL LB with kanamycin and carbenicillin as antibiotics and grown overnight at 37 °C. Unlabeled proteins were obtained by using the 50ml LB starter culture to inoculate 1 L LB. Isotopically ^{15}N and $^{15}N/^{13}C$ labeled proteins were obtained by pelleting the 50 mL LB starter culture, and using it to inoculate a 1 L M9 minimal media with 1 g/L of ^{15}N-ammonium chloride (Isotec) and/or 2 g/L of ^{13}C-glucose (Isotec). Cells were grown at 37 °C until the A_{600} was ~ 0.6 to 0.8, induced with 1 mM isopropyl-β-D-thiogalactopyranoside and cell growth was continued at 15 °C overnight in a shaker-incubator to a final A_{600} ~2.0. Cells were harvested by centrifugation and resuspended in 30 mL binding buffer (500 mM NaCl, 20 mM Tris-HCl, 5 mM imidazole, pH 8.0). For protein purification, cells were sonicated in the presence of ~300 μl of 1 mM phenylmethylsulfonyl fluoride. Cellular debris was removed by centrifugation of the cell lysate and 600 μl of 5% polyethyleneimine was added to the supernatant to precipitate the nucleic acids. Following centrifugation, the supernatant was loaded onto a Ni^{2+}-affinity column (Sigma), that was previously treated with 35 mL water, 35 ml 50mM $NiSO_4$ and 35 ml binding buffer. The Ni^{2+}-column was washed with 100 ml of binding buffer and the fusion proteins were eluted using ~60 mL of elution buffer (250 mM imidazole, 500 mM NaCl, 20 mM Tris, pH 8.0). The purified fusion protein fractions were combined and dialyzed overnight at room temperature in 1 L of TEV buffer (50mM Tris, 0.5 mM EDTA, 1mM DTT, 20 mM NaCl, pH 8.0) in the presence of 250 uL of 0.06 mM recombinant TEV protease [45]. The digested protein mixture was dialyzed again in I L binding buffer. The digest was loaded onto a Ni^{2+}-affinity column, which retained the GB1 tag and eluted the purified proteins. After TEV protease digestion, all LcrV and LcrG protein constructs used herein retained a three-residue cloning artifact “GHM” at their N-termini. Purified proteins were dialyzed in NMR buffer (10 mM $NaPO_4$, 10 mM NaCl, pH 7.0) and concentrated using Amicon Ultra 3K (Millipore). Protein concentrations were estimated by absorbance at A_{280}.

Site-directed mutations were generated using the Stratagene QuickChange kit. LcrV spanning residues 28-322 in a C273S background mutation was expressed and purified as described previously [18]. ^{15}N amino acid specific labeling of isoleucine and phenylalanine was done following a published protocol [46].

ILV labeling

Specific ^{13}C-labeling of the methyl groups of isoleucine (**I**), leucine (**L**) and valine (**V**) in LcrG and LcrV was done using ^{13}C-labeled α-keto acids as precursors following published

protocols [47]. The Cδ1 methyl group of isoleucine was ^{13}C-labeled by using 2-keto-3-(methyl-^{13}C)-butyric acid-4-^{13}C (Isotec # 571334); whereas the two leucine Cδ and the two valine Cγ methyl groups were ^{13}C-labeled by using 2-keto-3-(methyl-^{13}C)-butyric acid-4-^{13}C (Isotec # 571334). The α-keto acids were added to the minimal media when cell growth reached an A_{600} of 0.4 ~ 0.5. After 45–60 minutes the cultures were induced with 1.0 mM IPTG and cell growth was continued in a 15 °C shaker incubator overnight. Cells were harvested the following morning and proteins were purified as described above. LcrG* was ILV-labeled whereas LcrV was only labeled with the isoleucine ^{13}Cδ1 methyl group. The isoleucine ^{13}Cδ1 and the two valine ^{13}Cγ methyl groups of LcrG* were assigned by mutagenesis using alanine point mutations (in I20, I37, I47, I56, I67, and V44) and 2D ^{1}H-^{13}C HSQC spectrum of ILV-labeled LcrG was acquired for each mutant.

CD spectroscopy

Samples for circular dichroism spectroscopy contained 1–2 μM protein samples in buffer (10 mM $NaPO_4$, 10 mM NaCl, pH 7.0). CD spectra were acquired in triplicate using a JASCO J-815 Spectropolarimeter. Wavelength scans were collected at 20 °C at a scan rate of 50 nm/min. Thermal denaturation curves were monitored at 222 nm at a temperature ramp rate of 2 °C/min.

NMR Spectroscopy

NMR data were acquired at 25 °C using a Bruker Avance 800 MHz spectrometer equipped with a cryogenic triple resonance probe, processed with NMRPipe [48], and analyzed by NMRView [49]. Two-dimensional ^{1}H-^{15}N HSQC spectra [50] were acquired using 0.5–0.8 mM of protein samples. For backbone assignments of LcrG, ^{15}N/^{13}C LcrG* (0.9 mM) was used to acquire 2D ^{1}H-^{15}N HSQC, 3D HNCA, 3D HNCACB, and 3D CBCA(CO)NHA[50–52] datasets. Secondary structures were identified from the Cα, and Cβ chemical shifts [28]. To assign the backbone resonances of LcrG in the complex, ^{15}N/^{13}C LcrG* (0.6 mM) was complexed with unlabeled LcrV at a molar ratio of 1:1.2 and 2D ^{1}H-^{15}N HSQC [50], 3D HNCA and 3D HNCACB [52] were acquired.

NMR backbone dynamics

Backbone ^{15}N relaxation parameters (R_1, R_2, and steady-state heteronuclear {^{1}H}-^{15}N NOE) were acquired using a 0.7 mM ^{15}N LcrG* sample in NMR buffer. The steady-state heteronuclear {^{1}H}-^{15}N NOE was acquired as described in [53] with 2048 (^{1}H) * 128 (^{15}N) complex points, 60 scans per point and a 5 sec recycle delay. The heteronuclear {^{1}H}-^{15}N NOE was calculated as the ratio of intensities of each peak in the two 2D datasets [53]. Error bars were estimated using the standard deviation of the background signal of each spectrum. The ^{15}N backbone relaxation rates R_1 and R_2 were acquired as described [54]. The time delays used to determine R_1 were 10, 60, 120, 240, 400, 900 and 1100 ms, and the time delays used to determine R_2 were 20, 40, 50, 60, 70, 90, 100, 120 and 150 ms. Peak intensities were obtained using NMRView [49] and fitted using GNUPLOT [55]. Deviations from fitting were reported as error bars. Due to peak overlap, residues 9, 47, 64, 33, 36, 27, 28, 15, 42 and 70 were not used in the analysis. Residues 15, 54 and 61 could not be resolved, and hence were not used in the analysis.

NMR chemical shift mapping

Protein samples were dialyzed in the same NMR buffer and 2D ^{1}H-^{15} N HSQC spectra were acquired for ^{15}N-labeled samples and 2D ^{1}H-^{13}C HSQC spectra were acquired for ^{13}C-methyl-labeled samples. ^{15}N-labeled LcrG* (0.2 mM) was titrated with increasing amounts of unlabeled LcrV in molar ratios of 1:0, 1:0.5, 1:1.2, 1:2, 1:3, 1:4 and 1:6.5. Likewise, ^{13}C-ILV labeled LcrG* (0.36 mM) was titrated with increasing amounts of unlabeled LcrV in molar ratios of 1:0, 1:0.25, 1:0.5, 1:1 and 1:2. Additionally, isoleucine $^{13}C\delta1$-labeled LcrV (0.36 mM) was titrated with unlabeled LcrG* or unlabeled $LcrG^{FL}$ C34S in molar ratios of 1:0, 1:0.25, 1:0.5, 1:1 and 1:2.

Yop secretion assay

LcrG expression vectors were electroporated into the *lcrG* deletion mutant *Y. pestis* KIM5-3001.5. This strain contains an in-frame non-polar deletion of plasmid pCD1 sequences encoding LcrG residues 39 to 53 or LcrG(Δ39-53). This mutant secretes the Yop effector proteins constitutively in the presence and absence of calcium (calcium blind phenotype) and can be complemented back to the wild type calcium-regulated secretion phenotype by providing *lcrG* in trans. The LcrG proteins were expressed from a pBAD18 vector, induced with 0.2% L-(+)-arabinose upon shifting the temperature from 27 °C to 37 °C and normalized using the optical density (OD_{620}) of the cultures at harvest. Fractions were collected after 5 hours incubation at 37 °C. Levels of YopM in both whole cells and culture supernatant were analyzed by immunoblotting with anti YopM polyclonal antibodies. The levels of LcrG were also monitored in whole cells by immunoblotting with anti LcrG antibodies. LcrG C34S, LcrG C34A, and several mutants of the LcrG 52-73 region (deletion mutants Δ52-57, Δ58-62, Δ63-67, Δ68-73, Δ52-73; and point mutants I56N, K57E, K57L, R61E, R61L, L63N, I67N, K68E, and K68L) were tested by the Yop secretion assay.

Supplementary Material

Refer to Web version on PubMed Central for supplementary material.

Acknowledgments

Supported by NIH grants AI101823 (G.V.P), AI074856 (R.N.D.), and P30GM110761 (University of Kansas BioNMR Core Facility). We are grateful to Dr. Asokan Anbanandam for technical assistance in the NMR experiments.

Abbreviations

NMR	nuclear magnetic resonance
LcrG*	LcrG residues 7-73 C34S
$LcrG^{FL}$	full length LcrG
T3SS	type III secretion system

References

1. Cornelis GR. *Yersinia* type III secretion: send in the effectors. J Cell Biol. 2002; 158:401–408. [PubMed: 12163464]
2. Cornelis GR. The *Yersinia* Ysc-Yop 'type III' weaponry. Nat Rev Mol Cell Biol. 2002; 3:742–752. [PubMed: 12360191]
3. Burkinshaw BJ, Strynadka NC. Assembly and structure of the T3SS. Biochim Biophys Acta. 2014; 1843:1649–1663. [PubMed: 24512838]
4. Chatterjee S, Chaudhury S, McShan AC, Kaur K, De Guzman RN. Structure and biophysics of type III secretion in bacteria. Biochemistry. 2013; 52:2508–2517. [PubMed: 23521714]
5. Galan JE, Lara-Tejero M, Marlovits TC, Wagner S. Bacterial type III secretion systems: specialized nanomachines for protein delivery into target cells. Annu Rev Microbiol. 2014; 68:415–438. [PubMed: 25002086]
6. Cornelis GR. The type III secretion injectisome. Nat Rev Microbiol. 2006; 4:811–825. [PubMed: 17041629]
7. Mueller CA, Broz P, Muller SA, Ringler P, Erne-Brand F, Sorg I, et al. The V-antigen of *Yersinia* forms a distinct structure at the tip of injectisome needles. Science. 2005; 310:674–676. [PubMed: 16254184]
8. DeBord KL, Lee VT, Schneewind O. Roles of LcrG and LcrV during type III targeting of effector Yops by *Yersinia enterocolitica*. J Bacteriol. 2001; 183:4588–4598. [PubMed: 11443094]
9. Matson JS, Nilles ML. LcrG-LcrV interaction is required for control of Yops secretion in *Yersinia pestis*. J Bacteriol. 2001; 183:5082–5091. [PubMed: 11489861]
10. Fields KA, Nilles ML, Cowan C, Straley SC. Virulence role of V antigen of Yersinia pestis at the bacterial surface. Infect Immun. 1999; 67:5395–5408. [PubMed: 10496922]
11. Nilles ML, Williams AW, Skrzypek E, Straley SC. *Yersinia pestis* LcrV forms a stable complex with LcrG and may have a secretion-related regulatory role in the low-Ca^{2+} response. J Bacteriol. 1997; 179:1307–1316. [PubMed: 9023216]
12. Lawton DG, Longstaff C, Wallace BA, Hill J, Leary SE, Titball RW, et al. Interactions of the type III secretion pathway proteins LcrV and LcrG from *Yersinia pestis* are mediated by coiled-coil domains. J Biol Chem. 2002; 277:38714–38722. [PubMed: 12107165]
13. Matson JS, Nilles ML. Interaction of the *Yersinia pestis* type III regulatory proteins LcrG and LcrV occurs at a hydrophobic interface. BMC Microbiol. 2002; 2:16. [PubMed: 12102728]
14. Hamad MA, Nilles ML. Roles of YopN, LcrG and LcrV in controlling Yops secretion by *Yersinia pestis*. Adv Exp Med Biol. 2007; 603:225–234. [PubMed: 17966419]
15. Straley SC, Plano GV, Skrzypek E, Haddix PL, Fields KA. Regulation by Ca^{2+} in the *Yersinia* low-Ca^{2+} response. Mol Microbiol. 1993; 8:1005–1010. [PubMed: 8361348]
16. Skrzypek E, Straley SC. LcrG, a secreted protein involved in negative regulation of the low-calcium response in *Yersinia pestis*. J Bact. 1993; 175:3520–3528. [PubMed: 8501055]
17. Sarker MR, Sory MP, Boyd AP, Iriarte M, Cornelis GR. LcrG is required for efficient translocation of Yersinia Yop effector proteins into eukaryotic cells. Infect Immun. 1998; 66:2976–2979. [PubMed: 9596775]
18. Chaudhury S, Battaile KP, Lovell S, Plano GV, De Guzman RN. Structure of the *Yersinia pestis* tip protein LcrV refined to 1. 65 Å resolution. Acta Crystallogr Sect F. 2013; 69:477–481.
19. Derewenda U, Mateja A, Devedjiev Y, Routzahn KM, Evdokimov AG, Derewenda ZS, et al. The structure of *Yersinia pestis* V-antigen, an essential virulence factor and mediator of immunity against plague. Structure. 2004; 12:301–306. [PubMed: 14962390]
20. Pallen MJ, Dougan G, Frankel G. Coiled-coil domains in proteins secreted by type III secretion systems. Mol Microbiol. 1997; 25:423–425. [PubMed: 9282753]
21. Blocker AJ, Deane JE, Veenendaal AK, Roversi P, Hodgkinson JL, Johnson S, et al. What's the point of the type III secretion system needle? Proc Natl Acad Sci USA. 2008; 105:6507–6513. [PubMed: 18458349]

22. Basu A, Das U, Dey S, Datta S. PcrG protects the two long helical oligomerization domains of PcrV, by an interaction mediated by the intramolecular coiled-coil region of PcrG. BMC Struct Biol. 2014; 14:5. [PubMed: 24460624]
23. McGuffin LJ, Bryson K, Jones DT. The PSIPRED protein structure prediction server. Bioinformatics. 2000; 16:404–405. [PubMed: 10869041]
24. Kiss RS, Kay CM, Ryan RO. Amphipathic alpha-helix bundle organization of lipid-free chicken apolipoprotein A-I. Biochemistry. 1999; 38:4327–4334. [PubMed: 10194351]
25. Lau SY, Taneja AK, Hodges RS. Synthesis of a model protein of defined secondary and quaternary structure. Effect of chain length on the stabilization and formation of two-stranded alpha-helical coiled-coils. J Biol Chem. 1984; 259:13253–13261. [PubMed: 6490655]
26. Choy N, Raussens V, Narayanaswami V. Inter-molecular coiled-coil formation in human apolipoprotein E C-terminal domain. J Mol Biol. 2003; 334:527–539. [PubMed: 14623192]
27. Wang Y, Boudreaux DM, Estrada DF, Egan CW, StJeor SC, De Guzman RN. NMR structure of the N-terminal coiled-coil domain of the Andes hantavirus nucleocapsid protein. J Biol Chem. 2008; 283:28297–28304. [PubMed: 18687679]
28. Wishart DS, Nip AM. Protein chemical shift analysis: a practical guide. Biochem Cell Biol. 1998; 76:153–163. [PubMed: 9923684]
29. Kim MK, Kang YK. Positional preference of proline in alpha-helices. Protein Sci. 1999; 8:1492–1499. [PubMed: 10422838]
30. Eliezer D, Yao J, Dyson HJ, Wright PE. Structural and dynamic characterization of partially folded states of apomyoglobin and implications for protein folding. Nat Struct Biol. 1998; 5:148–155. [PubMed: 9461081]
31. Bax A, Spera S. Empirical Correlation between Protein Backbone Conformation and Cα and Cβ ^{13}C Nuclear Magnetic Resonance Chemical Shifts. J Am Chem Soc. 1991; 113:5490–5492.
32. Chen L, Balabanidou V, Remeta DP, Minetti CA, Portaliou AG, Economou A, et al. Structural instability tuning as a regulatory mechanism in protein-protein interactions. Mol Cell. 2011; 44:734–744. [PubMed: 22152477]
33. Rodgers L, Gamez A, Riek R, Ghosh P. The type III secretion chaperone SycE promotes a localized disorder-to-order transition in the natively unfolded effector YopE. J Biol Chem. 2008; 283:20857–20863. [PubMed: 18502763]
34. Zhong D, Lefebre M, Kaur K, McDowell MA, Gdowski C, Jo S, et al. The *Salmonella* type III secretion system inner rod protein PrgJ is partially folded. J Biol Chem. 2012; 287:25303–25311. [PubMed: 22654099]
35. Salomon D, Guo Y, Kinch LN, Grishin NV, Gardner KH, Orth K. Effectors of animal and plant pathogens use a common domain to bind host phosphoinositides. Nat Commun. 2013; 4:2973. [PubMed: 24346350]
36. Weise CF, Login FH, Ho O, Grobner G, Wolf-Watz H, Wolf-Watz M. Negatively charged lipid membranes promote a disorder-order transition in the Yersinia YscU protein. Biophys J. 2014; 107:1950–1961. [PubMed: 25418176]
37. Chen L, Ai X, Portaliou AG, Minetti CA, Remeta DP, Economou A, et al. Substrate-activated conformational switch on chaperones encodes a targeting signal in type III secretion. Cell Rep. 2013; 3:709–715. [PubMed: 23523349]
38. Hamada D, Kato T, Ikegami T, Suzuki KN, Hayashi M, Murooka Y, et al. EspB from enterohaemorrhagic *Escherichia coli* is a natively partially folded protein. FEBS J. 2005; 272:756–768. [PubMed: 15670156]
39. Babu MM, van der Lee R, de Groot NS, Gsponer J. Intrinsically disordered proteins: regulation and disease. Curr Opin Struct Biol. 2011; 21:432–440. [PubMed: 21514144]
40. Wright PE, Dyson HJ. Linking folding and binding. Curr Opin Struct Biol. 2009; 19:31–38. [PubMed: 19157855]
41. Lee PC, Stopford CM, Svenson AG, Rietsch A. Control of effector export by the *Pseudomonas aeruginosa* type III secretion proteins PcrG and PcrV. Mol Microbiol. 2010; 75:924–941. [PubMed: 20487288]

42. Perry RD, Straley SC, Fetherston JD, Rose DJ, Gregor J, Blattner FR. DNA sequencing and analysis of the low-Ca^{2+}-response plasmid pCD1 of *Yersinia pestis* KIM5. Infect Immun. 1998; 66:4611–4623. [PubMed: 9746557]
43. Huth JR, Bewley CA, Jackson BM, Hinnebusch AG, Clore GM, Gronenborn AM. Design of an expression system for detecting folded protein domains and mapping macromolecular interactions by NMR. Protein Sci. 1997; 6:2359–2364. [PubMed: 9385638]
44. Zhou P, Wagner G. Overcoming the solubility limit with solubility-enhancement tags: successful applications in biomolecular NMR studies. J Biomol NMR. 2010; 46:23–31. [PubMed: 19731047]
45. Geisbrecht BV, Bouyain S, Pop M. An optimized system for expression and purification of secreted bacterial proteins. Protein Expr Purif. 2006; 46:23–32. [PubMed: 16260150]
46. Wang Y, Nordhues BA, Zhong D, De Guzman RN. NMR characterization of the interaction of the *Salmonella* type III secretion system protein SipD and bile salts. Biochemistry. 2010; 49:4220–4226. [PubMed: 20397637]
47. Tugarinov V, Kanelis V, Kay LE. Isotope labeling strategies for the study of high-molecular-weight proteins by solution NMR spectroscopy. Nat Protoc. 2006; 1:749–754. [PubMed: 17406304]
48. Delaglio F, Grzesiek S, Vuister GW, Zhu G, Pfeifer J, Bax A. NMRPipe: a multidimensional spectral processing system based on UNIX pipes. J Biomol NMR. 1995; 6:277–293. [PubMed: 8520220]
49. Johnson BA. Using NMRView to visualize and analyze the NMR spectra of macromolecules. Methods Mol Biol. 2004; 278:313–352. [PubMed: 15318002]
50. Grzesiek S, Bax A. The importance of not saturating H_2O in protein NMR. Application to sensitivity enhancement and NOE measurements. J Am Chem Soc. 1993; 115:12593–12594.
51. Grzesiek S, Bax A. Correlating backbone amide and side chain resonances in larger proteins by multiple relayed triple resonance NMR. J Am Chem Soc. 1992; 114:6291–6293.
52. Wittekind M, Mueller L. HNCACB, a high sensitivity 3D NMR experiment to correlate amide proton and nitrogen resonances with the alpha-carbon and beta-carbon resonances in proteins. J Magn Reson. 1993; 101B:201–205.
53. Stone MJ, Fairbrother WJ, Palmer AG III, Reizer J, Saier MH Jr, Wright PE. Backbone dynamics of the Bacillus subtilis glucose permease IIA domain determined from ^{15}N NMR relaxation measurements. Biochemistry. 1992; 31:4394–4406. [PubMed: 1316146]
54. Farrow NA, Muhandiram R, Singer AU, Pascal SM, Kay CM, Gish G, et al. Backbone dynamics of a free and phosphopeptide-complexed Src homology 2 domain studied by ^{15}N NMR relaxation. Biochemistry. 1994; 33:5984–6003. [PubMed: 7514039]
55. Williams, T.; Kelley, C. Gnuplot 4.4: an interactive plotting program. 2010. http://gnuplot.sourceforge.net/
56. Thompson JD, Higgins DG, Gibson TJ. CLUSTAL W: improving the sensitivity of progressive multiple sequence alignment through sequence weighting, position-specific gap penalties and weight matrix choice. Nucleic Acids Res. 1994; 22:4673–4680. [PubMed: 7984417]

Research Highlights

- LcrG-LcrV interaction is important in the pathogenesis of *Yersinia pestis.*
- The atomic structure of the LcrG protein family is unknown.
- NMR shows that LcrG is a partially folded alpha helical protein.
- NMR identified a C-terminal region of LcrG that binds tightly to LcrV.

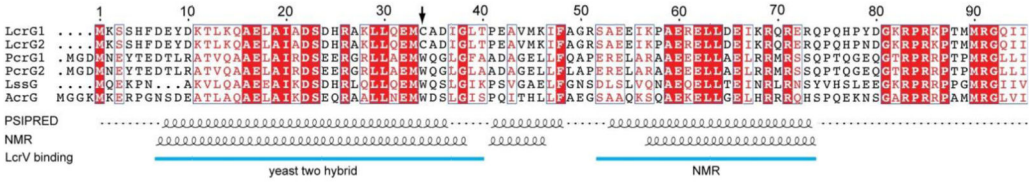

Fig. 1.

Sequence alignment of LcrG family of T3SS tip chaperones. The predicted helical regions by PSIPRED [23] are shown as well as the helical regions identified by NMR. Solid blue lines indicate the regions of tight-binding interaction with LcrV identified by yeast two hybrid [13] and by NMR. The proteins used in the alignment by CLUSTALW [56] are LcrG (*Yersinia pestis*), LcrG (*Yersinia enterocolitica*), PcrG (from two strains of *Pseudomonas aeruginosa*), LssG (*Photorhabdus asymbiotica*) and AcrG (*Aeromonas hydrophila*).

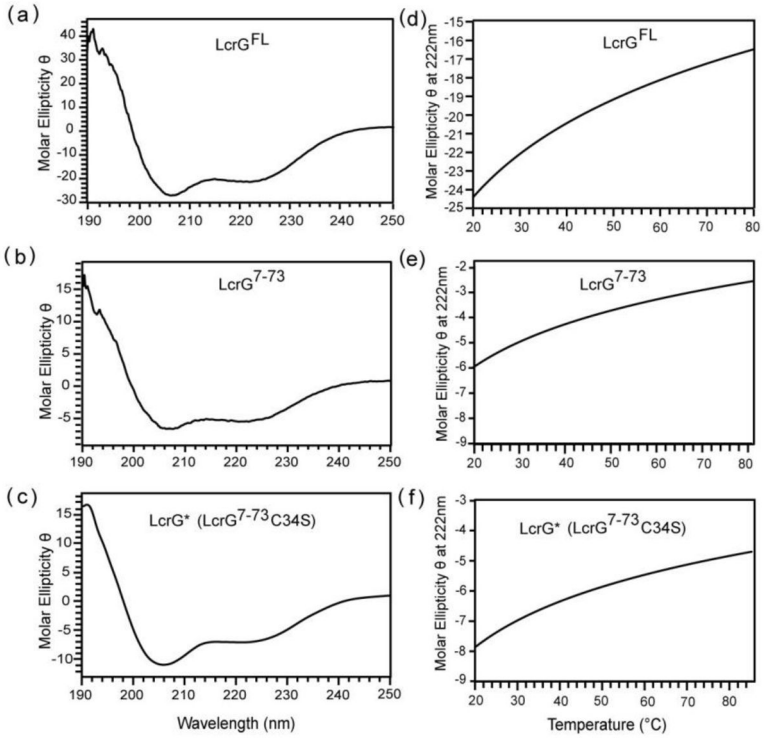

Fig. 2.

CD and thermal denaturation spectra of the various LcrG constructs. CD spectra were acquired for (a) $LcrG^{FL}$, (b) $LcrG^{7-73}$, and (c) LcrG* ($LcrG^{7-73}$ C34S). Thermal denaturation plots of (d) $LcrG^{FL}$, (e) $LcrG^{7-73}$, and (f) LcrG*. (Molar ellipticity θ = (deg·cm^2·dmol^{-1}) ×10^{-5}).

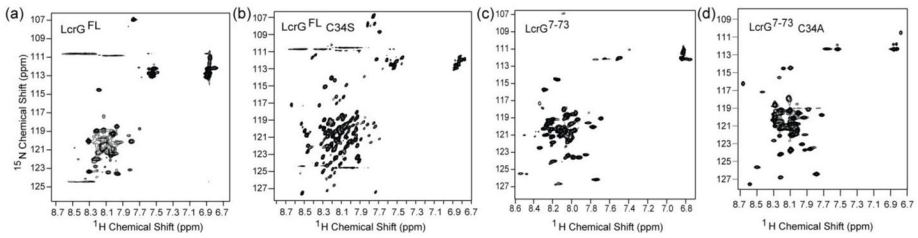

Fig. 3.

Two-dimensional ^{1}H-^{15}N HSQC spectra of (a) LcrG^{FL} (b) LcrG^{FL} C34S, (c) LcrG$^{7-73}$ and (d) LcrG$^{7-73}$ C34A, and (e) LcrG* (LcrG$^{7-73}$ C34S).

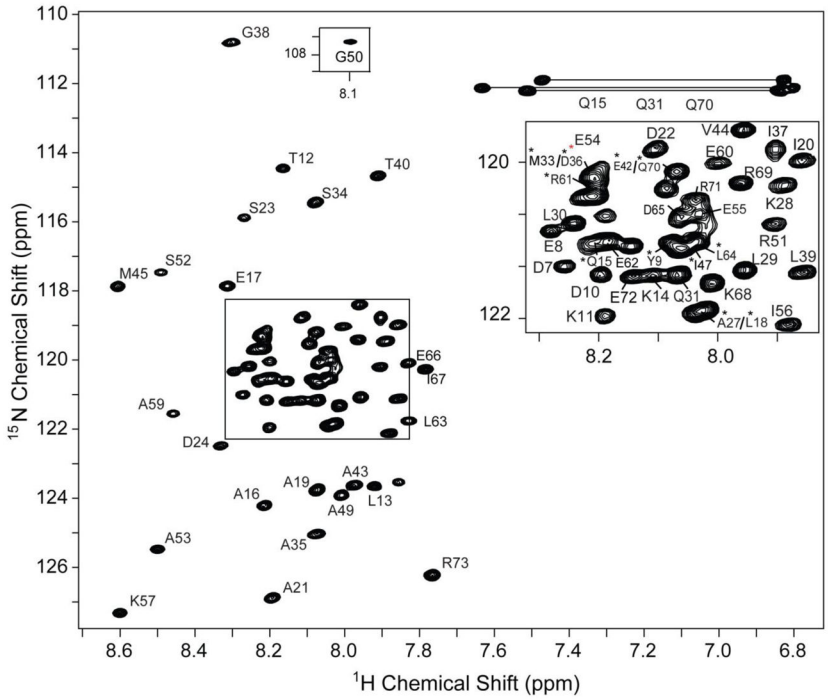

Fig. 4.

Assigned 2D ^{1}H-^{15}N HSQC spectrum of LcrG*. Overlapped peaks are marked with asterisk. The intensity for the peak of E54 is weak, its position is indicated by '+'.

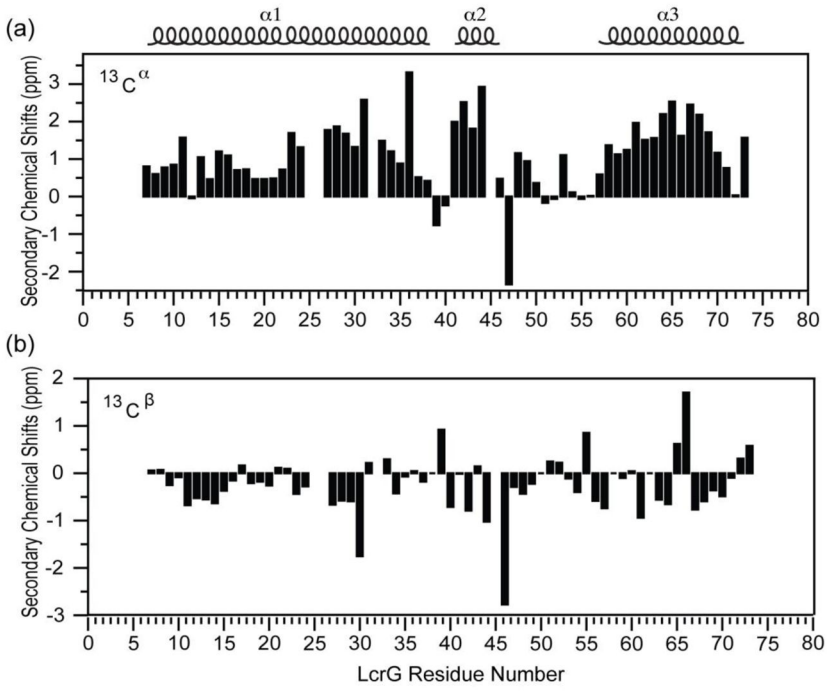

Fig. 5.

Secondary (a) $^{13}C\alpha$ and (b) $^{13}C\beta$ chemical shifts of LcrG*. Helical regions identified by the secondary chemical shifts are indicated.

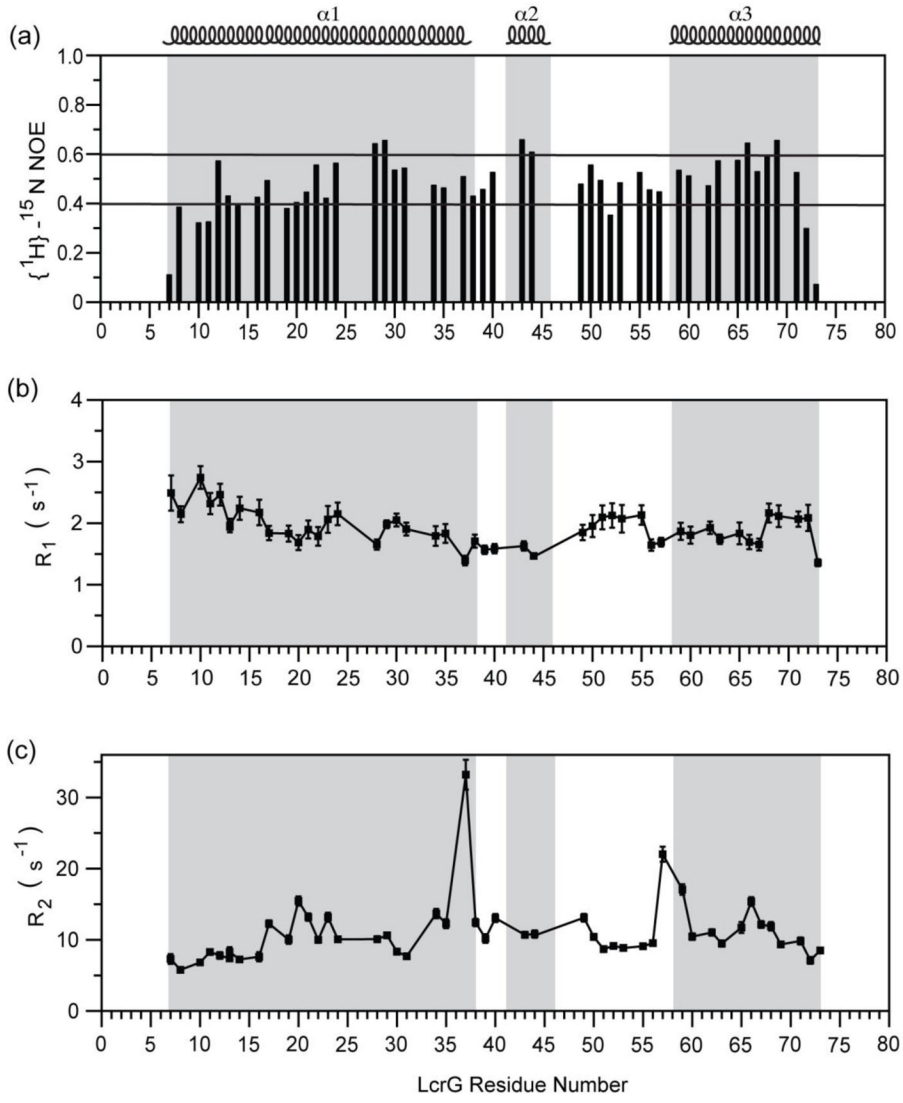

Fig. 6.

Backbone dynamics of LcrG*. (a) Heteronuclear $\{^1H\}$-^{15}N NOEs, and relaxation rates (b) R_1 and (c) R_2 for LcrG*. The helical regions are shaded. Gaps in the data are due to overlapped peaks or missing assignments.

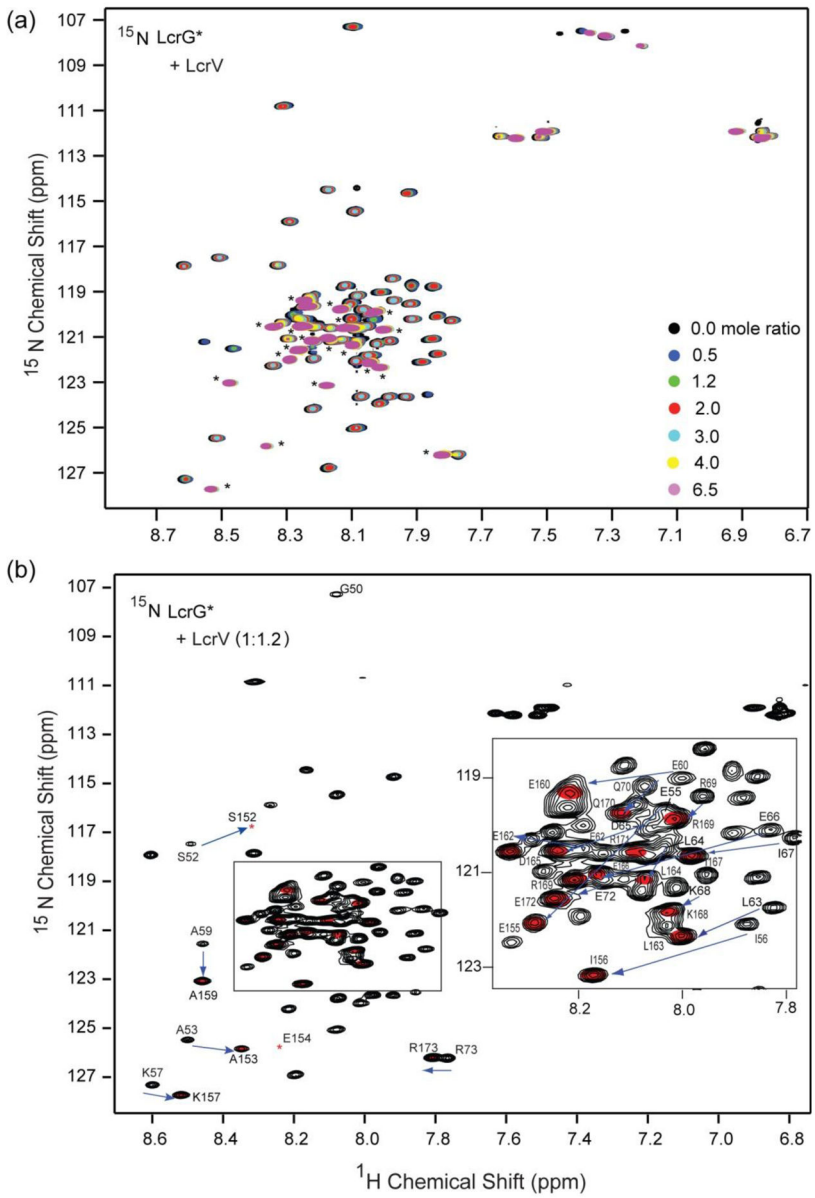

Fig. 7.

NMR titrations of ^{15}N LcrG* with LcrV. (a) Seven overlaid 2D ^{1}H-^{15}N HSQC spectra of LcrG* with increasing molar ratios of LcrV. Backbone amide peaks that appeared in new positions upon complex formation are marked with asterisks. The rest of the backbone amide peaks showed significant reduction in peak intensities. (b) Assigned 2D ^{1}H-^{15}N HSQC spectrum of the LcrG*-LcrV complex. Backbone amide peaks of residues S52 to R73 appeared in new positions upon complex formation. The original peak positions of these residues are indicated. Blue arrows point to the new peak positions (shown in red). The prefix “1” has been added to indicate LcrG residue number in complex with LcrV. The red asterisks indicate the complex peaks for S52 and E54 whose intensities were too low to appear on the contour level of the spectrum shown.

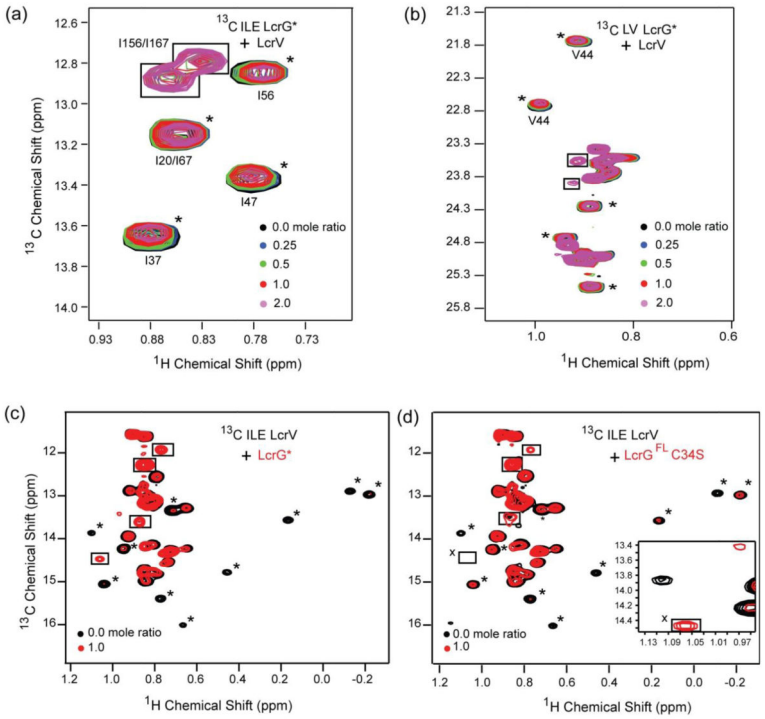

Fig. 8.

Titrations of ^{13}C ILV-labeled LcrG* with LcrV showing the ^{13}C methyl region of (a) isoleucine (ILE), and (B) leucine and valine (LV). The prefix “1” has been added to indicate LcrG residue number in complex with LcrV. The assignment of the complex peaks of I56 and I67 presented in (a) are based on the exchange behavior observed for ^{1}H/^{15}N correlations. Titrations of ^{13}C isoleucine-labeled LcrV with (c) LcrG* and (d) full length LcrG C34S. Slow exchange peaks are boxed and intermediate exchange peaks are marked with asterisk. A slow exchange peak in (d), marked ‘x’, has weak intensity and appears at a lower contour lever shown in the insert.

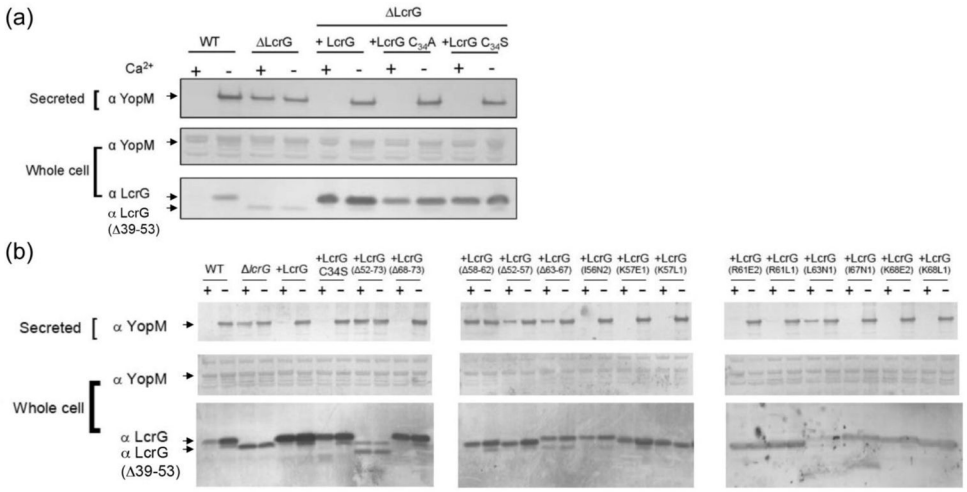

Fig. 9.

Effect of LcrG mutations on YopM secretion in the presence or absence of Ca^{2+}. Wild type *Y. pestis* KIM5-3001, the *lcrG* deletion strain KIM5-3001.5 (Δ*lcrG*) and KIM5-3001.5 (Δ*lcrG*) carrying plasmid pBAD-LcrG (+LcrG), or derivatives of this plasmid carrying point mutations (panels a and b) or small deletions (panel b) in *lcrG* were grown for 1 h at 27 °C and for 5 h at 37 °C in the presence (+) or absence (−) of 2.5 mM $CaCl_2$. Secreted and whole cell proteins were analyzed by SDS-PAGE and immunoblotting with LcrG or YopM antibodies (α). The location of the YopM, LcrG and LcrG(Δ39-53) bands are indicated by arrowheads.